

promoting access to White Rose research papers



Universities of Leeds, Sheffield and York
<http://eprints.whiterose.ac.uk/>

White Rose Research Online URL for this paper:
<http://eprints.whiterose.ac.uk/2640>

Published paper

Mullis, A.M. (2007) *Understanding the formation of twinned dendrites ('feather' grains)*. In: Solidification Processing 07 Proceedings of the 5th Decennial International Conference on Solidification Processing, 23-25 July, Sheffield, UK.

Understanding the formation of twinned dendrites ('feather' grains)

A.M. Mullis

Institute for Materials Research, University of Leeds, Leeds LS2 9JT, UK

Abstract

The phenomenon of feather grain growth is interesting from both a theoretical and commercial point of view. Here we report the results of phase-field simulations aimed at understanding the formation of twinned dendrites. We show that, while a competition between oppositely directed capillary and kinetic anisotropies with a simple four-fold symmetry can produce low anisotropy structures such as dendritic seaweed, there is no indication that this can give rise to twinned dendrites. In contrast, adding small components of an anisotropy, with higher order harmonics, can produce features reminiscent of twinned dendrites and may also be able to stabilise the grooved tip morphology.

Keywords: Twinned dendritic growth, feather growth.

1. Introduction

Due to their deleterious properties, the formation of 'feather' grains is a significant problem in the DC casting of commercial Al alloys [1]. Crystallographic investigations by Henry *et al.* [2,3] have shown that feather grains are twinned dendritic structures the formation of which also involves a change in growth direction from $\langle 100 \rangle$ to $\langle 110 \rangle$ with a $\{111\}$ twin plane. In Al-Mg alloy, $\langle 110 \rangle$ dendrites have also been observed growing without twin assistance [4]. In one of only a few systematic studies, Morris and Ryvola [5] found that a minimum solute concentration is required for feather grain growth. It has been suggested [6] that this is because the effect of solute addition is to cause grain refinement, and that twinning occurs only after a certain degree of grain refinement has been achieved. A number of authors have also found that high imposed thermal gradients tend to favour feather grain growth [7].

Despite the importance of dendritic twins in industrial casting practice, there is no general consensus as to the morphology of a twinned dendrite. Wood *et al.* [6] have argued that a stable morphology would be for the dendrite to display a sharper than normal tip with the twin plane emanating from the point. Conversely, Henry *et al.* [3] have suggested that a twin dendrite would display a split or grooved tip with the twin plane running down the trunk from the grove (Figure 1).

A number of cubic systems undergo a change in growth direction from $\langle 100 \rangle$ through $\langle 110 \rangle$ to $\langle 111 \rangle$ as the growth velocity is increased; in particular, this has been observed *in situ* in the $\text{NH}_4\text{Cl-H}_2\text{O}$ system [8]. This behaviour may be due to competition between the surface energy anisotropy which favours $\langle 100 \rangle$ growth at low velocity and the kinetic anisotropy which favours $\langle 111 \rangle$ growth at high velocity [9]. Such a competition might also stabilise the grooved tip dendrite morphology.

Recent years have seen great advances in the understanding of crystal growth kinetics from the study of undercooled melts. However, such fruitful studies have not proved possible on Al-alloys, partly because Al_2O_3 is a good heterogeneous nucleant. The observation that feather grains can also be formed in some Cu alloys [10] suggests that Cu is a potentially suitable analogue for Al.

Velocity-undercooling relationships and microstructural evolution in Cu-x wt%Sn ($x = 1, 2, 3, 4$) alloy have been studied by Dragnevski *et al.* [11,12], with at least three different growth regimes being identified. At the very low undercoolings associated with conventional casting, solidification proceeded by growth along the $\langle 100 \rangle$ direction. As the undercooling was increased, a change in the growth direction from $\langle 100 \rangle$ to $\langle 111 \rangle$ was observed, with a likely $\langle 110 \rangle$ intermediate also present. Moreover, X-ray texture analysis revealed that, in the 2 and 3 wt% alloys, the $\langle 111 \rangle$ dendrites were growing via a twin assisted mechanism, confirming a previous observation of twinning in the 3 wt% alloy [13]. Finally, at high undercooling, there was a change back to the $\langle 100 \rangle$ growth direction, with no evidence of

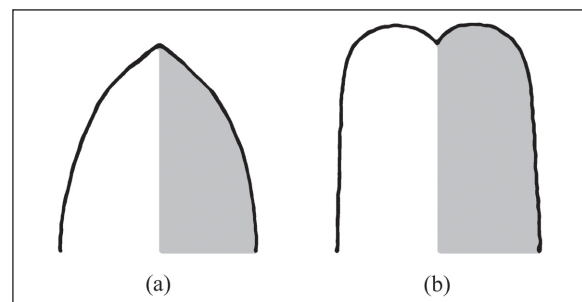


Figure 1: Schematic illustration of the (a) pointed and (b) grooved tip morphologies suggested for twinned dendrites.

twinning being present. In all these systems this transition back to <100> growth occurred over a very narrow range of undercoolings ($85 < \Delta T < 90$ K). Equivalent experiments performed on high purity Cu showed that the <100> growth direction was preserved at all undercoolings, with no change in the preferred growth direction or twinning being evident.

Experiments reveal that twinned and untwinned growth are identified by distinct velocity-undercooling relationships, each of which is a simple power-law (Figure 2). By extrapolating the growth velocity relationships it is clear that the fastest growing mode is always the one that dominates.

The results of these studies are thus consistent with the known facts for feather-grain formation, even if the mechanism giving rise to the morphology is not understood. A minimum solute concentration is required to induce either a change in the growth direction or dendrite twinning, with both <111> growth and twinning being restricted to an intermediate range of growth velocities. However, what role the solute plays in bringing about either a change the growth direction or initiating twinning is unknown. It is, however, clear from the work of Dragnevski *et al.* that twinning is unrelated to grain refinement, with many of their twinned samples containing only a single grain.

It is clear from the ideas of Henry *et al.* [3] that any model of dendritic twinning should incorporate capillary and kinetic anisotropies which can be independently varied in magnitude and direction. It is also apparent both from industrial experience and our own experiments that solute plays an important role, with neither a change in growth direction nor dendritic twinning being observed in pure melts.

In this paper, we use a phase-field model of solidification in a binary alloy to study the effect of competing capillary and kinetic anisotropy and to determine whether such a competition could lead to one of the morphologies proposed for a twinned dendrite.

2. Computational method

Our investigation was conducted using the binary model of Warren and Boettinger [14], wherein, for the case of isothermal solidification in an ideal solution between components A and B, this leads to transport and anisotropic phase-equations given respectively by

$$\dot{c} = \nabla \cdot D_c \left[\nabla c + \frac{v_m}{R} c(1-c)(H^B - H^A) \nabla \phi \right] \quad (1)$$

and

$$\frac{\dot{\phi}}{M_\phi} = \left[\varepsilon^2(\theta) \nabla^2 \phi - (1-c)H^A - cH^B \right] - \frac{\partial}{\partial x} \left(\varepsilon(\theta) \varepsilon'(\theta) \frac{\partial \phi}{\partial y} \right) + \frac{\partial}{\partial y} \left(\varepsilon(\theta) \varepsilon'(\theta) \frac{\partial \phi}{\partial x} \right) + \nabla \cdot (\varepsilon^2(\theta) \nabla \phi). \quad (2)$$

where ϕ is the phase variable taking values 0 in the solid and 1 in the liquid, c is the concentration of solute (chemical species B) in the solvent and ε is related to the width of the diffuse interface, δ by

$$\varepsilon^2 = \frac{6\sqrt{2}\sigma^A \delta^A}{T_m^A} = \frac{6\sqrt{2}\sigma^B \delta^B}{T_m^B} \quad (3)$$

Here, D_c is the effective diffusivity, σ is the interfacial energy between the solid and liquid phases, T_m is the

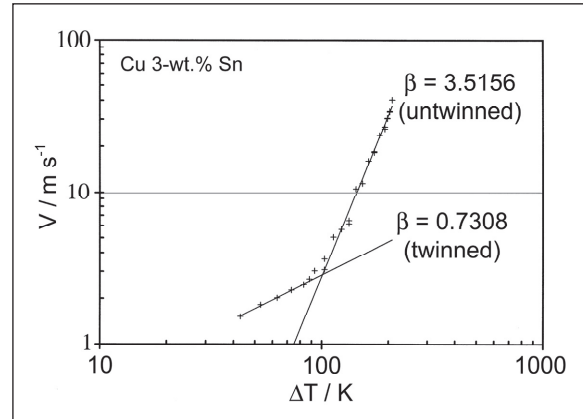


Figure 2: Velocity vs. undercooling curves for Cu-3 wt%Sn alloy of the form $V \propto (\Delta T)^\beta$ [from Ref. 11].

melting temperature, v_m is the molar mass and R the gas constant. The superscripts A and B indicate that the specified quantity refers to the pure substances A and B respectively. Note that Equation 3 implies that, if σ and T_m for each of the species A and B are assigned fixed (i.e. physical) values, it is not possible to independently vary both δ^A and δ^B . The terms $H^{A,B}$ are defined in [14].

The kinetic mobility is given by

$$M_\phi = (1-c)M^A + cM^B \quad (4)$$

with

$$M^{A,B} = \frac{(T_m^{A,B})^2 \beta^{A,B}}{6\sqrt{2}L^{A,B} \delta^{A,B}} \quad (5)$$

where β is the kinetic coefficient for interface attachment, and L is the latent heat per unit volume.

Anisotropy is introduced by writing [15]

$$\varepsilon(\theta) = \bar{\varepsilon} \eta(\theta) = \bar{\varepsilon}(1 + \gamma \cos k\theta) \quad (6)$$

where γ is the anisotropy strength and k is a mode number, which for cubic metals will be 4.

In common with a number of other formulations of the phase-field problem, the effect of Equation 6 is to introduce anisotropy into the interface width. It can be shown by an asymptotic analysis in the limit of vanishing interface width, that the effect of introducing anisotropy into the width of the diffuse interface is to introduce physical anisotropies in both the surface energy and the kinetics of attachment at the interface, the magnitudes and directions of which would normally be coupled [16].

One approach to decoupling the surface energy and kinetic anisotropies is to assume that the characteristic time scale, τ , is also a function of angle [17–19]. However, recently we have demonstrated [20] that, by introducing a complex anisotropy function, η , the anisotropies can be decoupled even in those phase-field models in which only the interface width is assumed anisotropic.

$$\eta(\theta) = 1 + \gamma_r \cos k_r \theta + i \gamma_i \cos k_i (\theta + \theta_0) \quad (7)$$

Here γ_r and γ_i are the amplitudes of the real and imaginary components of the anisotropy, k_r and k_i are the corresponding mode numbers and θ_0 is an offset angle. An asymptotic analysis in the limit $\delta \rightarrow 0$ reveals that the capillary anisotropy, with strength γ_d is a function of γ_r only,

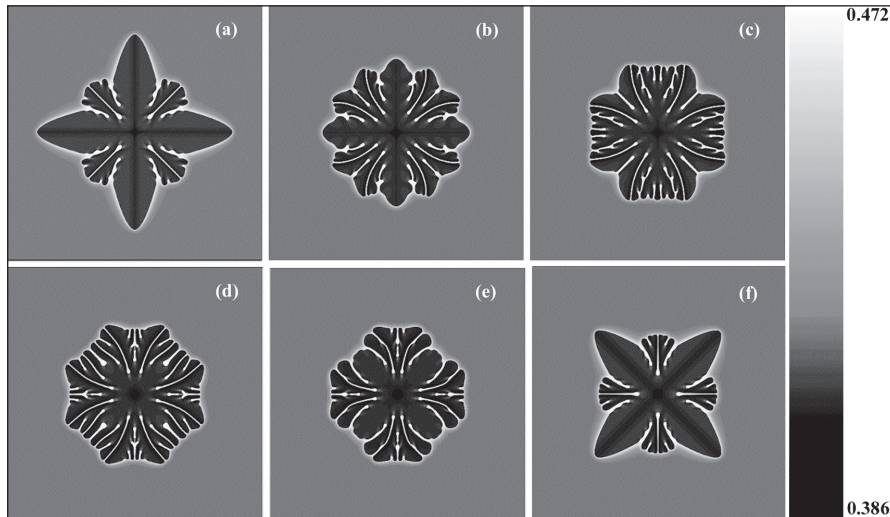


Figure 3: Solute map for alloy solidification with a competition between capillary anisotropy (direct towards the sides of the box) and kinetic anisotropy (directed towards the corners of the box), for $\gamma_k/\gamma_d = 0.083, 0.117, 0.133, 0.166, 0.183$ and 0.217 .

while the kinetic anisotropy with strength γ_k is a function of γ_r and γ_i , permitting the desired decoupling. Incidentally, for pure four-fold symmetric capillary and kinetic anisotropies, we require $k_r = 4$ but $k_i = 2$.

3. Results

Figure 3 shows a sequence of simulations in which γ_k has been varied at fixed γ_d , producing a competition between the capillary and kinetic anisotropies. The computational parameters used in all the simulations reported here are characteristic of the Ni-Cu system and are given in [21]. As reported elsewhere, the formulation of the phase-field problem used here is equivalent to assuming an ideal solution between the two end member compositions, giving a simple ‘lens’ type phase diagram. The liquidus temperature for this solution at the (far-field) concentration studied, $c_o = 0.408$, is 1594.5 K and the melting interval is 24 K. The dimensionless undercooling for this system $(T - T_l)/(T_s - T_l)$ is thus ≈ 0.85 . All simulations were run on at least two meshes differing in resolution by a factor of $\sqrt{2}$.

The solute boundary layer in the simulations is clearly visible, with the highest concentrations being observed in the residual liquid channels between the dendrite arms and/or ‘seaweed’ channels. All of the frames are taken after the same model time. In this particular set of simulations, the capillary anisotropy, with magnitude $\gamma_d = 0.30$, is directed towards the sides of the bounding box, with the kinetic anisotropy being directed towards the corners.

With increasing kinetic anisotropy, capillary dendrites (a) shrink back and kinetic doublons emerge (b). ‘Dendritic seaweed’ structures are observed in the regime where the two competing anisotropies are approximately equal (c) and (d) before the emergence of kinetic dendrites (e) which eventually dominate, leaving remnant capillary doublons (f).

Clearly, such competition can result in a low effective anisotropy, giving rise to morphologies such as doublons. Boettinger *et al.* [22] have speculated that doublons may play an important role in the formation of feather grains and indeed, frozen in dendritic seaweed and doublons have been observed directly in deeply undercooled Cu [23]. There is, however, no evidence of dendrites propagating with a steady-state grooved tip as the result of competition between simple four-fold symmetric anisotropies.



Figure 4: Solidification morphology resulting from growth under a composite four-fold + eight-fold anisotropy.

Consequently, we have also looked at the effect of introducing higher order components to the anisotropy and have found that even small higher order components can have a profound influence on growth morphologies, a point first noted by Alain Karma. In particular, for a system which has predominantly a four-fold symmetry with minor components of higher harmonics of a four-fold symmetry we may write

$$\eta(\theta) = 1 + \sum_{m=1}^n \gamma_r^{(m)} \cos 4m\theta + i\gamma_i^{(m)} \cos 2m(\theta + \theta_0) \quad (8)$$

The growth morphology that results is distinctly different from the standard dendritic morphology, as is shown in Figure 4, where we have used the anisotropy with $n = 2$, $\gamma_r^{(1)} = 0.02$, $\gamma_r^{(2)} = -0.0007$ and $\gamma_i^{(1)} = \gamma_i^{(2)} = 0$. That is, the model has a predominantly four-fold symmetry in both the capillary and kinetic anisotropies with a small, *opposing*, eight-fold component superimposed.

$\gamma_r^{(1)} = 0.02$ is a relatively large anisotropy and four well-developed primary dendrites should result. Instead we observe doublon-like channels running along the primary trunk,

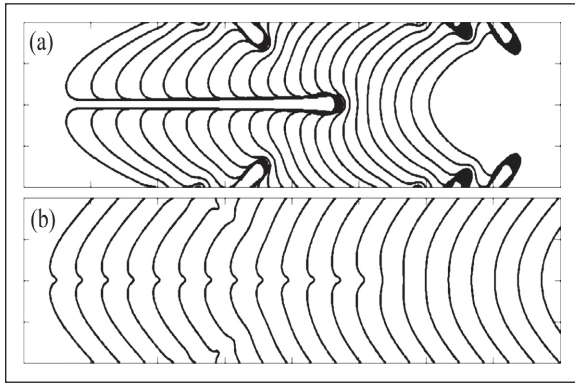


Figure 5: Composite contour maps of (a) the tip of a doublon and (b) the tip of a dendrite with a steady state groove. Growth direction is from right to left.

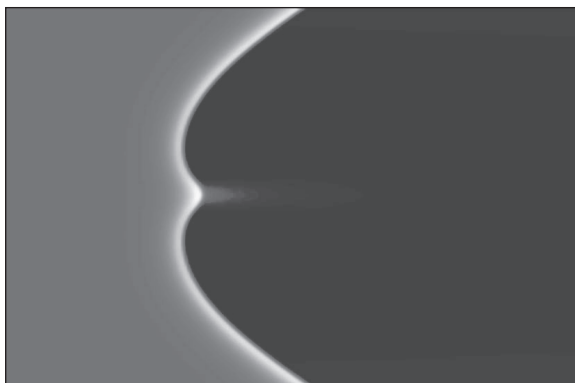


Figure 6: Solute map in the tip region of a 'grooved tip dendrite'.

although the trunks themselves have a far greater degree of regularity than we would expect of doublons resulting from growth under low anisotropy. Although still not a twin, this morphology now has a far greater superficial resemblance to the twin dendrite morphology than the 'seaweed' structure above. In particular, analogies might be drawn between a straight twin boundary and the central doublon channel and between a wavy twin boundary and the residual liquid channels occurring between the dendrite side arms. As a result of this simulation, we believe that anisotropy components with higher order symmetry play an important role in the stabilisation of the grooved tip morphology.

This idea is supported by the following simulations, produced during an investigation into the implicit anisotropy introduced by the regularity of the finite difference mesh. Figure 5a shows a simulation of a doublon growing under 'normal' low anisotropy conditions. The early frames (towards the right of the Figure) show that the tip is unstable and is increasing in radius. At a critical curvature the tip flattens and develops a bifurcation. Following bifurcation, the two 'tip' branches rapidly outgrow the 'trough', thus developing the narrow channel along the trunk characteristic of the doublon morphology. The early evolution of the feature in Figure 5b appears similar. The tip is unstable and its radius is increasing. At a critical curvature, the tip flattens and again develops a bifurcation. However, in this case, a stable groove is developed which is then propagated along with the dendrite in a steady-state fashion, resulting in a morphology at the dendrite tip akin to that proposed by Henry *et al.* [3]. A detailed view of the tip region is shown in Figure 6.

However, exactly why the morphology shown in Figure 5b is stable is not clear; this morphology was produced by a simulation in which the parameter space had been chosen so as to exaggerate the implicit anisotropy so that the phenomenon could be studied [21]. What is clear though is that the mesh-induced anisotropy does not have a simple four-fold symmetry. In fact, when the dominant four-fold component of the mesh induced anisotropy was removed a small 16-fold symmetric component was revealed (note that due to the process used to remove the four-fold component of the implicit anisotropy we cannot tell whether an eight-fold component was present, although it would seem likely that it was).

4. Summary and Conclusions

Despite their importance in industrial casting practice, dendritic twins are a solidification microstructure about which surprisingly little is known and for which no convincing theoretical model has been proposed. Henry *et al.* [3] speculated that twinned dendrites have a split or grooved tip, but without proposing any rigorous theoretical framework in which this could be established. In this paper we have reported some preliminary phase-field results which show that the grooved tip morphology can indeed propagate as a stable solidification morphology and appears to be stabilised by, an as yet uncharacterised, superposition of four-fold symmetric and higher order components of the anisotropy.

References

1. D.A. Granger and J. Liu, *JOM*, June 1983, p. 54.
2. S. Henry, T. Minghetti and M. Rappaz, *Acta Mater.*, **46** (1998) 6431.
3. S. Henry, P. Jarry and M. Rappaz, *Metall. Mater. Trans. A*, **29A** (1998) 2807.
4. S. Henry and M. Rappaz, in: 'Solidification and Gravity 2000', *Mater. Sci. Forum*, **329** (2000) 65.
5. L.R. Morris and M. Ryvola, *Microstr. Sci.*, **9** (1981) 141.
6. H.J. Wood, J.D. Hunt and P.V. Evans, *Acta Mater.*, **45** (1997) 569.
7. J.A. Eady and L.M. Hogan, *J. Cryst. Growth*, **23** (1974) 129.
8. K.A. Jackson and K.A. Gudge, *J. Cryst. Growth*, **225** (2001) 264.
9. S.K. Chan, H.H. Reimer and M. Kahlweit, *J. Cryst. Growth*, **32** (1976) 303.
10. A. Kamio, *Proc. Japan-US Cooperative Science Program Seminar on Solidification Processing of Advanced Materials*, Otsu, Kanagawa, Japan, 1989, p. 195.
11. K.I. Dragnevski, R.F. Cochrane and A.M. Mullis, *Metall. Mater. Trans. A*, **35** (2004) 3211.
12. A.M. Mullis, K.I. Dragnevski and R.F. Cochrane, *Mater. Sci. Eng. A*, **375-377** (2004) 547.
13. S.E. Battersby, R.F. Cochrane and A.M. Mullis, *J. Mater. Sci.*, **35** (2000) 1365.
14. J.A. Warren and W.J. Boettinger, *Acta Metall. Mater.*, **43** (1995) 689.
15. A.A. Wheeler, B.T. Murray and R.J. Schaefer, *Physica D*, **66** (1993) 243.
16. A.A. Wheeler, W.J. Boettinger and G.B. McFadden, *Phys. Rev. A*, **45** (1992) 7424.
17. G. Caginalp, *Phys. Rev. A*, **39** (1989) 5887.
18. O. Penrose and P.C. Fife, *Physica D*, **43** (1990) 44.
19. R. Kobayashi, *Physica D*, **63** (1993) 410.
20. A.M. Mullis, *Europhys. J. B*, **41** (2004) 377.
21. A.M. Mullis, *Comput. Mater. Sci.*, **36** (2006) 345.
22. W.J. Boettinger *et al.*, *Acta Mater.*, **48** (2000) 43.
23. K.I. Dragnevski, R.F. Cochrane and A.M. Mullis, *Phys. Rev. Lett.*, **89** (2002) 215502. ■